

Biomimetic Antireflective Silicon Nanocones Array for Small Molecules Analysis

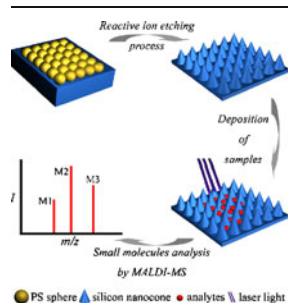
Yandong Wang,¹ Zhoufang Zeng,² Jie Li,³ Lifeng Chi,^{1,4} Xinhua Guo,² Nan Lu¹

¹State Key Laboratory of Supramolecular Structure and Materials, College of Chemistry, Jilin University, Changchun, People's Republic of China

²College of Chemistry, Jilin University, Changchun, People's Republic of China

³The Fourth Hospital of Jilin University, Changchun, People's Republic of China

⁴Physikalisches Institut und Center for Nanotechnology (CeNTech), Westfälische Wilhelms-Universität, Münster, Germany



Abstract. Biomimetic antireflective silicon nanocones array is used for analysis of small molecules by mass spectrometry. The role of the absorbed laser energy and its distribution in the laser desorption/ionization process has been investigated by varying the antireflective features precisely. By optimizing the antireflective silicon array, the absorbed laser energy can be channeled completely into the desorption/ionization of analytes. The optimized silicon array exhibits excellent performance to detect peptide, amino acid, drug molecule, and carbohydrate without any interference in the low-mass region.

Key words: Biomimetics, Biosensors, Photo absorption, Colloidal lithography, SALDI MS

Introduction

Matrix assisted laser desorption/ionization mass spectrometry (MALDI-MS) is a key method in the analysis of biological and synthetic macromolecules [1, 2]. However, some limits are associated with this method, including interference ions in the low mass region ($m/z < 700$ Da), the intolerance to salt, and random distribution of the hot spots due to the introduction of organic matrix in traditional MALDI method [3–6]. Therefore, surface assisted laser desorption/ionization mass spectrometry (SALDI-MS) has been developed as an alternative technique, which affords several advantages such as the ability to detect small molecules, easy sample preparation, low-noise background, and so on [7–10]. Usually, SALDI substrates refer to the two types: (1) inorganic bulk materials such as germanium [4], gold [11–14], silver [6, 15], silicon particles [16], and tungsten oxide [17]; (2) structured surfaces such as porous silicon [6, 18–22], zinc oxide nanowires [23], titania nanotubes [24], silicon microcolumns [25], or silicon nanowires [5, 26, 27] and silicon nanowells [9].

Electronic supplementary material The online version of this article (doi:10.1007/s13361-012-0498-4) contains supplementary material, which is available to authorized users.

Correspondence to: Nan Lu; e-mail: luenan@jlu.edu.cn

To clarify the laser desorption/ionization (LDI) process, various possible mechanisms of SALDI have been proposed, such as laser induced thermal desorption [6], laser induced surface restructuring/melting [8], optical absorption followed by transferring the laser energy into internal energy [19], as well as gas expansion [22, 28]. For the proposed mechanisms, one thing in common is that the laser energy absorbed by SALDI substrate is transferred to the analytes and makes the analyte vaporized and ionized. Therefore, high photo absorption has been considered as a vital role in leading to a successful desorption/ionization of analytes for a SALDI substrate [6, 7, 18, 22]. However, the effect of the absorbed laser energy and its dissipation and/or relaxation during the LDI process has rarely been reported because of the random morphologies of the SALDI substrate and the complexity of LDI process [28, 29]. For example, spot-to-spot variations in SALDI performance are inevitably caused by the random distribution of particles or structures [8, 28]. Therefore, it is desirable to perform LDI process on the ordered surface.

Recently, we demonstrated a method to fabricate biomimetic silicon nanocones (SiNC) array with the nanosphere masked reactive ion etching for suppressing the reflection [30, 31]. The antireflective structure could be applied for improving LDI performance because of the high photo absorption ability [6, 7]. More importantly, the gradual increase of the photo absorption can be obtained by varying the surface features such

Received: 9 August 2012

Revised: 5 September 2012

Accepted: 8 September 2012

Published online: 19 December 2012

as the height and period of the SiNC array, which makes it possible to investigate the effect of the absorbed laser energy and its dissipation and/or relaxation.

In this paper, the SiNC array is used as SALDI substrate for small molecules analysis. The role of the absorbed laser energy and its distribution in the laser desorption/ionization process has been investigated. The absorbed laser energy can be channeled completely into the desorption/ionization of analytes by optimizing the surface features of antireflective structure such as the height and period. The optimized SiNC array exhibits the excellent desorption/ionization performance for detecting peptide, amino acid, drug molecule, and carbohydrate with little or no interference in the low mass region. The detection limit of bradykinin is about 10 fmol with the signal to noise (S/N) ratio value of 11.39. The value of the linear regression R^2 of the calibration curve for the glucose in human urine sample is 0.9992. Furthermore, the practical application of this method is demonstrated by the successful analysis of glucose in urine sample from a diabetic patient.

Experimental Section

Chemicals and Materials

Bradykinin 1–7 fragment, arginine acids (Arg), polyethylene glycol (PEG), dihydroxybenzoic acid (DHB), α -cyano-4-hydroxycinnamic acid (CHCA), dithranol (DI), and the monodispersed polystyrene (PS) sphere with less than 5 % diameter variation used in the experiments were purchased from (Sigma-Aldrich, St. Louis, MO, USA). Drug molecule temozolomide (TMZ) was received as a gift from the School of Life Sciences, Jilin University, China. The urine samples of healthy man and diabetic patient were provided by the Fourth Clinical Hospital of Jilin University, Changchun, China. The Si wafers (n type [100]) were obtained from Youyan Guigu (Beijing, China). Ethanol, acetone, tetrahydrofuran, and chloroform were purchased from Guangfu Fine Chemical Research

Institute (Tianjin, China) in the highest available purity. Ultrapure water (18.2 M Ω ·cm) was used directly from a Millipore System (Marlborough, France). All solvents and chemicals were of reagent quality without further purification.

Assembly of Polystyrene (PS) Monolayer

The monolayer of PS nanospheres was prepared according to the reference [30, 31]. In brief, 0.2 mL solution of dispersed PS nanosphere in absolute ethanol was dropped on the surface of the water, and then the monolayer was transferred onto the silicon wafer; the monolayer of PS nanosphere was obtained.

Fabrication of SiNC Arrays

The SiNC array was fabricated by conducting reactive ion etching with the nanosphere monolayer as etching mask on a Plasmalab Oxford 80 plus (ICP65) system (Oxford Instrument Co., Bristol, UK) with the gaseous mixture of SF₆, CHF₃ and O₂.

Characterization

Scanning electron microscope (SEM) images were taken using environmental scanning electron microscope (ESEM, Model XL 30 ESEM FEG; Micro FEI Philips, Oregon, USA). The samples were sputtered with a thin layer of Pt prior to imaging (2 nm in thickness).

Sample Preparation for MS Analysis

The stock solution of PEG and TMZ was prepared by dissolving PEG and TMZ in Milli-Q (Marlborough, France) water with the concentration of 100 μ M, respectively. The solution of bradykinin 1–7 fragment with the concentration of 100 μ M was prepared by dissolving bradykinin in water containing 2.5 mM citric acid. The solution of Arg with the concentration of 100 μ M was prepared by dissolving Arg in acetic acid-ammonium acetate (pH=4.5) buffer solution.

Urine samples were collected from healthy and diabetic humans and diluted 20-fold in water without further

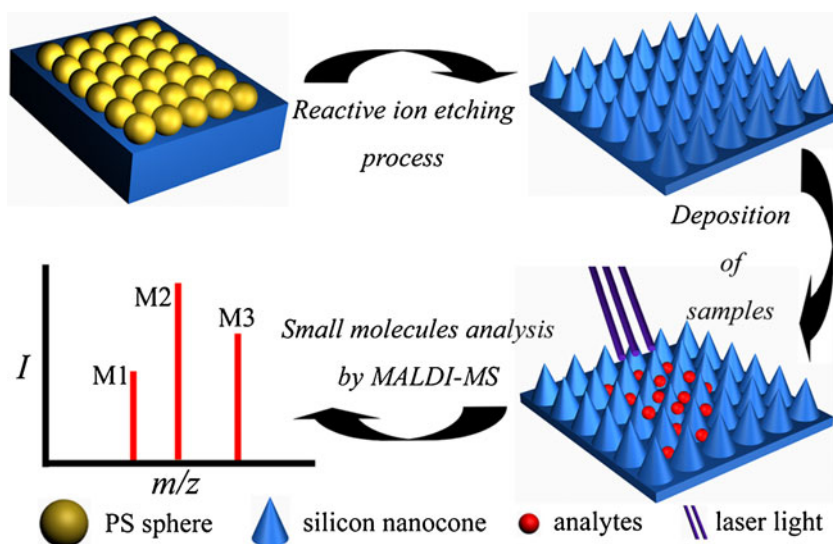


Figure 1. Schematic description of fabricating periodic SiNC array as SALDI substrate

treatment. During the quantification process, standard glucose (0.5–10 mM) was added into the diluted healthy human urine samples.

CHCA (10 mgmL⁻¹) was prepared for the detection of bradykinin 1–7 fragment and Arg by using the solution containing 50 % (vol/vol) ACN and 0.1 % (vol/vol) TFA. The solution of DHB (10 mgmL⁻¹) was prepared for the detection of PEG by using water as solvent. DI (10 mgmL⁻¹) was diluted in tetrahydrofuran for the analysis of TMZ. The sample and matrix were mixed at equal volume, which was deposited onto the MALDI sample plate and dried in the air.

The SiNC array substrates were firstly rinsed with ethanol and water, and dried by N₂. The clean substrates were attached onto a MALDI plate by adhesive polyimide tape. The *m/z* calibration has been performed by detecting the internal peptides using matrix on a polished silicon substrate. The sample solution (0.5–1.0 μL) was deposited onto the SiNC array and dried in air before SALDI-MS analysis.

MALDI-TOF MS experiment was performed in the linear mode on a Kratos Axima CFRplus spectrometer (Shimadzu Biotech, Manchester, UK) with a 337 nm nitrogen laser and acceleration voltage of 20 kV. 150 laser shots were used to obtain each spectrum.

Results and Discussion

Schematic description of the fabrication of SiNC array for SALDI substrate is shown in Figure 1. The fabrication method for preparing SiNC array has been described previously [30, 31]. Briefly, a monolayer of colloidal polystyrene (PS) spheres was initially assembled on a Si substrate, and then the Si substrate with the PS sphere array was subjected to the reactive ion etching process with a gaseous mixture of SF₆, CHF₃, and O₂. Finally, the etched Si nanostructure was cleaned by taking ultrasonication in acetone, chloroform, ethanol, and water in sequence for 3 min. The analyte solutions were deposited directly on the

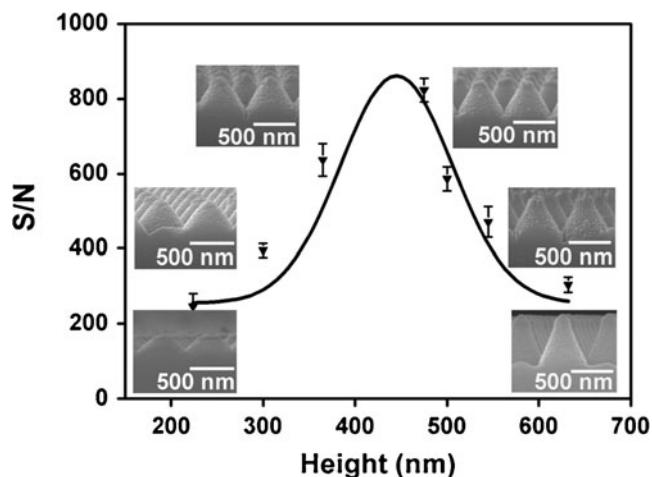


Figure 2. The dependence of signal-to-noise ratios of PEG on the height of cones ranging from 224 to 632 nm with the period of 580 nm

structured surface and dried in air at room temperature before MS measurements.

Different surface morphologies such as cavity, frustum of cone and cone can be obtained by adjusting the etching duration (Supplementary Figure S1), which allows us to investigate the impact of morphology on the LDI efficiency. Polyethylene glycol (PEG, MW: 1500, 10 pmol) was used as the model analyte to evaluate LDI performance of the silicon structures. The S/N ratio of PEG peaks is plotted as a function of etching duration, which indicates that the SiNC array exhibits the best desorption/ionization performance (Supplementary Figure S2).

To investigate the effect of the absorbed laser energy on the MS signals, the S/N ratios of PEG on the SiNC array with the period of 580 nm and heights ranging from 224 to 632 nm were collected and shown in Figure 2. For the SiNC array with the same period, LDI performance should be improved by increasing the height of cones because the corresponding photo absorption is increased (Supplementary

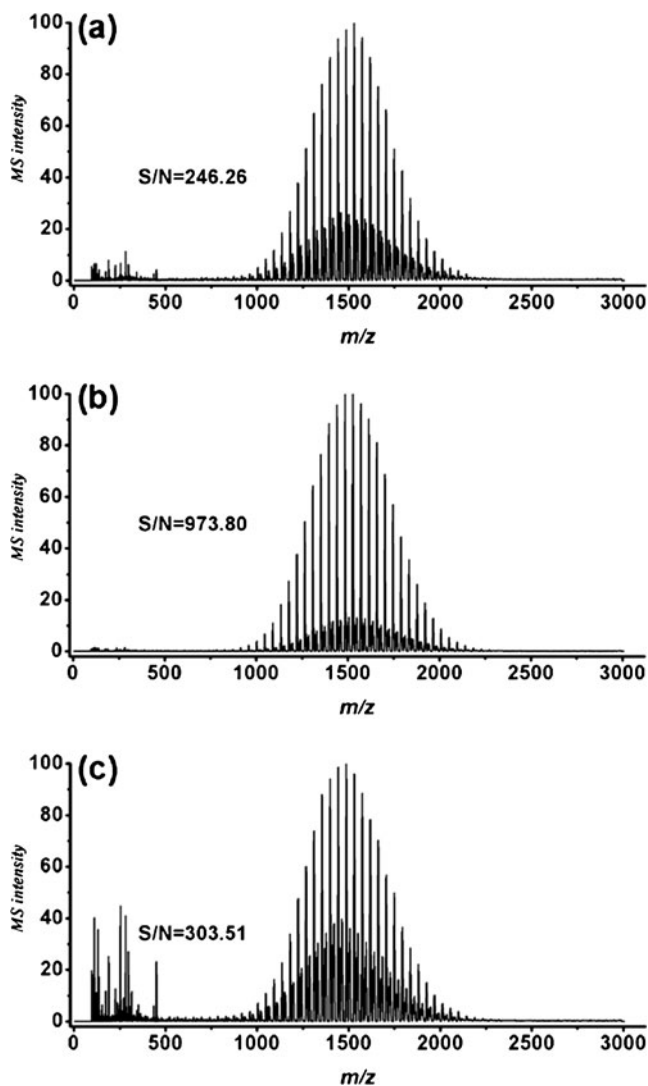


Figure 3. Mass spectra of PEG collected on the SiNC arrays with different heights (a) 224 nm, (b) 475 nm, and (c) 632 nm

Figure S3) [27, 32]. As shown in Figure 2, the S/N ratio of PEG peaks increases with increasing the height of SiNC array when the height is lower than 475 nm, which should be caused by the increment in the photo absorption and surface area, as well as the limited thermal conductivity [4–6, 26–28], however, it decreases with further increasing the height. It is speculated that the further increasing of height may result in the absorbed laser energy being used for dissociation of silicon skeleton, besides LDI of analyte, which leads to the decrease of the LDI performance.

Figure 3 shows the mass spectra of PEG obtained on the SiNC arrays with different heights. For the spectrum collected on SiNC array with height of 224 nm, as shown in Figure 3a, the peaks below 500 Da are assigned to silicon clusters because each pair of the neighboring peaks is disjoined by 28 Da, which is corresponding to the mass of Si atom (Supplementary Figure S4). The emergence of Si cluster peaks and the weak PEG peaks indicates that the efficiency of photo absorption and thermal activation of this SiNC array is limited. In contrast, the S/N ratio and the signal intensity of PEG peaks are significantly enhanced when the height of SiNC array is 475 nm, as shown in Figure 3b. Furthermore, the peaks of Si clusters disappear, which indicates that the absorbed laser energy was used effectively in desorption/ionization of analyte molecules. However, the peaks of Si clusters re-emerge and the signal intensity of PEG is decreased for the SiNC array with height of 632 nm (Figure 3c). It is worthy noting that the signal intensity of Si clusters peaks is five times higher than the one observed in Figure 3a, while the signal intensity of PEG peaks is comparable. It is suggested that more silicon skeletons are exposed directly under the laser light with the

height increasing. Part of the laser energy is dissipated in desorption/ionization of silicon skeletons rather than being effectively channeled into analyte ion production, resulted in the decrease of LDI efficiency. Therefore, the ion peaks of silicon clusters can be suppressed or eliminated by modulating the height of the SiNC array. The LDI efficiency of these SiNC array is not proportional to the increase of photo absorption ability.

When the height of SiNC array is constant, the photo absorption of SiNC array should vary with the periods, which were fabricated by using different sized PS spheres as etching mask. Figure 4 shows the mass spectra of PEG by using SiNC arrays with periods of 1100, 580, and 220 nm as substrate, respectively. The heights of these SiNC arrays are approximately 230 nm because the highest etching selectivity of PS sphere to silicon is about 1:1 in this work. The absorption of the SiNC array increases with decreasing the period when the height is fixed except for the first-order and second-order diffraction (Supplementary Figure S5). As shown in Figure 4, the peaks of silicon clusters and background noise are significantly suppressed and the intensity of PEG peaks is enhanced effectively by decreasing the period. In addition to the increased absorption, the reason might be that the thermal conductivity of a rough wafer is smaller than that of a smooth one [26–28]. Therefore, better desorption/ionization performance could be obtained by using silicon nanocones or nanopillars with small feature size and high aspect ratio, which can be fabricated by optimizing the etching conditions [33, 34]. The above results show that the distribution of the absorbed laser energy can be directly revealed from the variation of

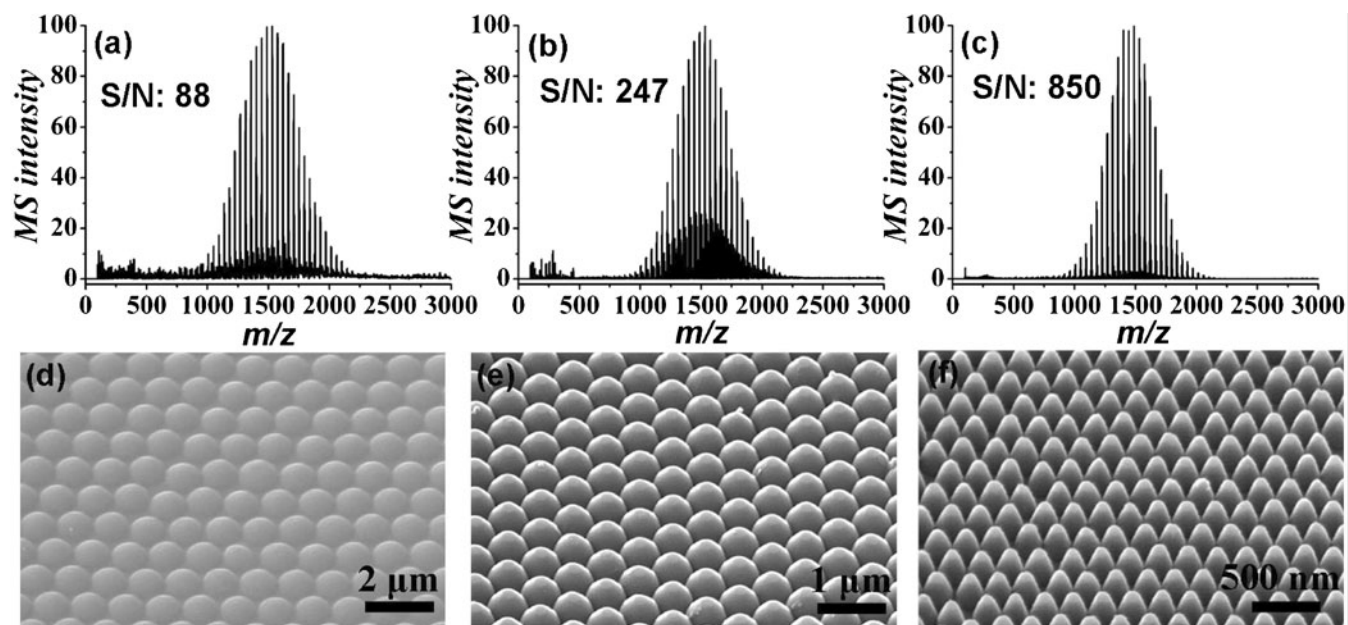


Figure 4. Mass spectra of PEG collected on the SiNC arrays with different periods (a) 1100 nm, (b) 580 nm, and (c) 220 nm. The corresponding SEM images are shown in panel (d), (e), and (f), respectively

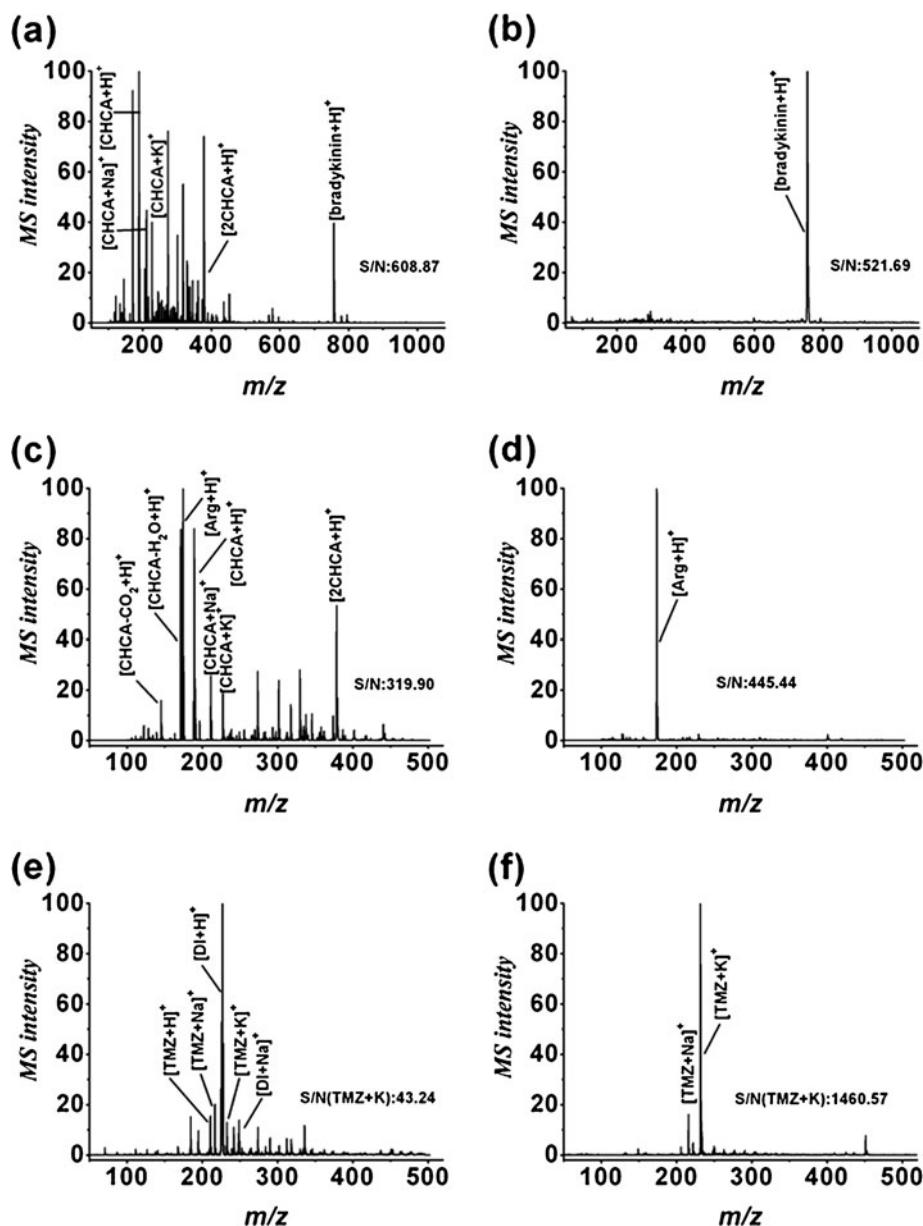


Figure 5. Mass spectra of bradykinin, Arg, and TMZ measured with the traditional MALDI technique (a), (c), (e) and by taking the SiNC array (height: 340 nm) as substrate (b), (d), (f), respectively. The concentration of analyte is 1 pmol

ions peaks in the mass spectrum. The concurrent increase in analyte ions signal and decrease in silicon cluster ions signal correlates to more efficient desorption/ionization process because the absorbed laser energy has been more effectively channeled into analyte ion production rather than silicon cluster ejection. The effective transfer of laser energy from the substrate to the analyte, rather than the high photo absorption ability, is the most important for the successful desorption/ionization process.

It is worth noting that the SiNC array with a height ranging from 300 to 500 nm also exhibits successful desorption/ionization of analytes (Figure 2). Therefore, the SiNC array with a height of 340 nm was used as a LDI substrate to detect peptide, amino acid and drug molecule in

comparison with the traditional MALDI analysis, as shown in Figure 5. The bradykinin peptide (m/z : 756.85) was tested because its ion peak position is far away from the interfering matrix peaks, allowing easy observation of the matrix and analyte ions peaks. High background noises dominate the spectrum generated from matrix related ions including [CHCA+H]⁺, [CHCA+Na]⁺, [CHCA+K]⁺ and [2CHCA+H]⁺ in the low-mass range (<500 Da), see Figure 5a. However, matrix ion peaks have been completely eliminated, and little or no fragmentation peak of the bradykinin can be observed (Figure 5b). This result indicates that a matrix-free LDI process can be achieved by using the SiNC array. Therefore, the Arginine (Arg) amino acid with mass lower than 500 Da (m/z : 174.20) has been detected by using the traditional

MALDI technique (Figure 5c) and the SiNC array (Figure 5d) to further evaluate the potential application of SiNC array in the analysis of small molecules. From Figure 5c, we can find that although Arg is desorbed/ionized as $[\text{Arg}+\text{H}]^+$ with a great intensity, various matrix ions peaks are observed which obscure the identification of analyte. As mass spectrum presented in Figure 5d when the SiNC array was applied, matrix ions interference disappears and only the protonated ion of Arg can be observed. As can be seen in Figure 5c, the Arg ion peak is distinguishable with the highest S/N ratio of 319.90 in the spectrum although with the matrix ions interference. However, the high density of matrix molecules in the plume may usually result in signal suppression of analytes [35]. For example, Figure 5e shows that the drug temozolomide (TMZ) molecule ions (m/z : 194.15) with a poor S/N ratio ($[\text{TMZ}+\text{K}]^+$: 43.24) are observed and buried in the interfering matrix ions by the traditional MALDI technique. In contrast, TMZ detected on the SiNC array exhibits strong MS signals and high S/N ratio (1460.57). The bradykinin solution with lower concentration was used to study the limit of detection (LOD) for the proposed SiNC array. When the concentration of the bradykinin solution is as low as 10 fmol, the bradykinin can be observed with a S/N ratio of 11.39, as shown in Figure S6. The above results demonstrate that the SiNC arrays exhibit excellent performance in the small molecules analysis without interference in the low-mass region. Therefore, the SiNC array is of great potential in the metabolomics study and drug discovery where high-throughput screening of small molecules is constantly required.

Quantitative analysis by MALDI-TOF MS has been considered as a great challenge due to the poor reproducibility of analyte signals [11]. The homogeneity achieved using ordered nanostructures for LDI process is higher than obtained by the formation of crystals of the analyte molecule with the conventional matrix, which results in an improvement in quantitative analysis. Glucose is ionized as the sodium ion adduct $[\text{M}+\text{Na}]^+$ and the potassium ion adduct $[\text{M}+\text{K}]^+$ at m/z 203 and 219 on the SiNC array with 475 nm in height after 0.5 and 10 mM glucose were spiked into the diluted healthy human urine samples, as shown in Figure 6a and b, respectively. Furthermore, the calibration curve derived from human urine solution containing glucose standards is shown in Figure 6c, in which the $[\text{M}+\text{Na}]^+$ signal intensity was used for quantification according to the reference [11]. The working curve extends from 0.5 to 10 mM of glucose with a linear regression R^2 value of 0.9992, which includes the upper limit of the healthy glucose concentration.

Additionally, the practical application of this method is tested by the analysis of glucose in urine sample from a diabetic patient. Supplementary Figure S7a displays the mass spectrum of the urine sample from a female type II diabetic patient who took the hypoglycemic drug without any chemical treatment. The ion peaks at m/z 203 and 219 corresponding to glucose are observed on the spectrum for

the urine of patient (Supplementary Figure S7a), while there is no visible glucose signal for the healthy man (Supplementary Figure S7b). Comparing the results from Supplementary Figure S7b, the unidentified ion peaks in Supplementary Figure S7a may be the metabolic products of hypoglycemic drug. It is worth noting that the MALDI technique can not show the glucose signal because of the high salt concentration in urine sample (data not shown). Moreover, the concentration of glucose calculated from Figure 6a is about 3.90 mM, which is close to the value 4.17 mM detected from the Fourth Clinical Hospital of Jilin

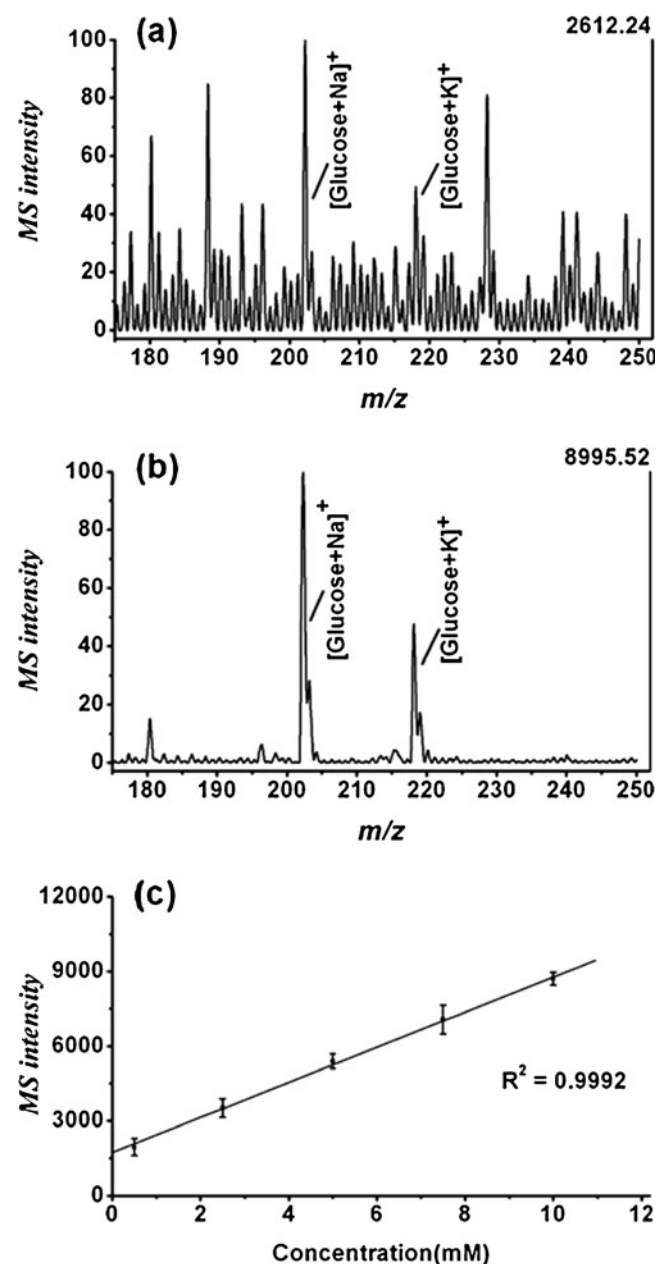


Figure 6. Mass spectra of glucose with concentration of (a) 0.5 mM and (b) 10 mM in human urine which has been diluted to 20-fold. (c) Working curve for the quantification of glucose in the range of 0.5–10 mM in human urine

University, Changchun, China. These results suggest that this method can provide a potentially precise and time-saving procedure for the quantitative assay of glucose in clinical studies.

Conclusions

In conclusion, biomimetic silicon nanocones array is used as the LDI substrate for small molecules analysis. The role of the absorbed laser energy and its distribution in the LDI process has been investigated by modulating the surface features. The distribution of the absorbed laser energy can be directly revealed from the variation of ions peaks in the mass spectrum. The concurrent increase in analyte ions signal and decrease in silicon cluster ions signal on the SiNC array correlates to more efficient desorption/ionization process because the absorbed laser energy has been more effectively channeled into analyte ion production rather than silicon cluster ejection. The optimized SiNC array exhibits excellent performance to detect peptide, amino acid, drug molecule, and carbohydrate with little or no interference in the low mass range. Quantitative analysis of glucose in human urine sample creates a calibration curve with a good linear regression R^2 value of 0.9992. Moreover, the glucose in real urine sample from a diabetic patient has been detected successfully with impressive intensity due to the low background ions in the low mass range. This method has the potential for applications in routine urine assay in clinical studies.

Acknowledgments

The authors are thankful to Lifeng Wang from Alan G. MacDiarmid Institute, Jilin University, for providing access to the MALDI-MS measurement. This work was supported by the National Basic Research Program (2009CB939701).

References

- Zeng, Z.F., Wang, Y.D., Shi, S.L., Wang, L.F., Guo, X.H., Lu, N.: On-plate selective enrichment and self-desalting of peptides/proteins for direct MALDI MS analysis. *Anal. Chem.* **84**, 2118–2123 (2012)
- Kailasa, S.K., Kiran, K., Wu, H.F.: Comparison of ZnS semiconductor nanoparticles capped with various functional groups as the matrix and affinity probes for rapid analysis of cyclodextrins and proteins in surface-assisted laser desorption/ionization time-of-flight mass spectrometry. *Anal. Chem.* **80**, 9681–9688 (2008)
- Hsu, N.F., Tseng, S.Y., Wu, C.Y., Ren, C.T., Lee, Y.C., Wong, C.H., Chen, C.H.: Desorption ionization of biomolecules on metals. *Anal. Chem.* **80**, 5203–5210 (2008)
- Seino, T., Sato, H., Yamamoto, A., Nemoto, A., Torimura, M., Tao, H.: Matrix-free laser desorption/ionization-mass spectrometry using self-assembled germanium nanodots. *Anal. Chem.* **79**, 4827–4832 (2007)
- Go, E.P., Apon, J.V., Luo, G.H., Saghatelian, A., Daniels, R.H., Sahi, V., Dubrow, R., Cravatt, B.F., Vertes, A., Siuzdak, G.: Desorption/ionization on silicon nanowires. *Anal. Chem.* **77**, 1641–1646 (2005)
- Kruse, R.A., Li, X.L., Bohn, P.W., Sweedler, J.V.: Direct assay of aplysia tissues and cells with laser desorption/ionization mass spectrometry on porous silicon. *Anal. Chem.* **73**, 3639–3645 (2001)
- Okuno, S., Arakawa, R., Okamoto, K., Matsui, Y., Seki, S., Kozawa, T., Tagawa, S., Wada, Y.: Requirements for laser-induced desorption/ionization on submicrometer structures. *Anal. Chem.* **77**, 5364–5369 (2005)
- Wada, Y., Yanagishita, T., Masuda, H.: Ordered porous alumina geometries and surface metals for surface-assisted laser desorption/ionization of biomolecules: Possible mechanistic implications of metal surface melting. *Anal. Chem.* **79**, 9122–9127 (2007)
- Gulbakan, B., Park, D., Kang, M.C., Kececi, K., Martin, C.R., Powell, D.H., Tan, W.H.: Laser desorption ionization mass spectrometry on silicon nanowell arrays. *Anal. Chem.* **82**, 7566–7575 (2010)
- Nayak, R., Knapp, D.R.: Matrix-free LDI mass spectrometry platform using patterned nanostructured gold thin film. *Anal. Chem.* **82**, 7772–7778 (2010)
- Su, C.L., Tseng, W.L.: Gold nanoparticles as assisted matrix for determining neutral small carbohydrates through laser desorption/ionization time-of-flight mass spectrometry. *Anal. Chem.* **79**, 1626–1633 (2007)
- Wu, H.P., Yu, C.J., Lin, C.Y., Lin, Y.H., Tseng, W.L.: Gold nanoparticles as assisted matrices for the detection of biomolecules in a high-salt solution through laser desorption/ionization mass spectrometry. *J. Am. Soc. Mass Spectrom.* **20**, 875–882 (2009)
- Castellana, E.T., Russell, D.H.: Tailoring nanoparticle surface chemistry to enhance laser desorption ionization of peptides and proteins. *Nano Lett.* **7**, 3023–3025 (2007)
- Teng, C.H., Ho, K.C., Lin, Y.S., Chen, Y.C.: Gold nanoparticles as selective and concentrating probes for samples in MALDI MS analysis. *Anal. Chem.* **76**, 4337–4342 (2004)
- Chiu, T.C., Chang, L.C., Chiang, C.K., Chang, H.T.: Determining estrogens using surface-assisted laser desorption/ionization mass spectrometry with silver nanoparticles as the matrix. *J. Am. Soc. Mass Spectrom.* **19**, 1343–1346 (2008)
- Wen, X.J., Dagan, S., Wysocki, V.H.: Small-molecule analysis with silicon-nanoparticle-assisted laser desorption/ionization mass spectrometry. *Anal. Chem.* **79**, 434–444 (2007)
- Yang, X.J., Hu, X.K., Loboda, A.V., Lipson, R.H.: Microstructured tungsten oxide: A generic desorption/ionization substrate for mass spectrometry. *Adv. Mater.* **22**, 4520–4523 (2010)
- Shen, Z.X., Thomas, J.J., Averbuj, C., Broo, K.M., Engelhard, M., Crowell, J.E., Finn, M.G., Siuzdak, G.: Porous silicon as a versatile platform for laser desorption/ionization mass spectrometry. *Anal. Chem.* **73**, 612–619 (2001)
- Luo, G.H., Chen, Y., Siuzdak, G., Vertes, A.: Surface modification and laser pulse length effects on internal energy transfer in DIOS. *J. Phys. Chem. B* **109**, 24450–24456 (2005)
- Northen, T.R., Yanes, O., Northen, M.T., Marrinucci, D., Uritboonthai, W., Apon, J., Gollidge, S.L., Nordstrom, A., Siuzdak, G.: Clathrate nanostructures for mass spectrometry. *Nature* **449**, 1033–1037 (2007)
- Arakawa, R., Shimomae, Y., Morikawa, H., Ohara, K., Okuno, S.: Mass spectrometric analysis of low molecular mass polyesters by laser desorption/ionization on porous silicon. *J. Mass Spectrom.* **39**, 961–965 (2004)
- Wei, J., Buriak, J.M., Siuzdak, G.: Desorption-ionization mass spectrometry on porous silicon. *Nature* **399**, 243–246 (1999)
- Shin, W.J., Shin, J.H., Song, J.Y., Han, S.Y.: Effects of ZnO nanowire length on surface-assisted laser desorption/ionization of small molecules. *J. Am. Soc. Mass Spectrom.* **21**, 989–992 (2010)
- Lo, C.Y., Lin, J.Y., Chen, W.Y., Chen, C.T., Chen, Y.C.: Surface-assisted laser desorption/ionization mass spectrometry on titania nanotube arrays. *J. Am. Soc. Mass Spectrom.* **19**, 1014–1020 (2008)
- Walker, B.N., Razunguzwa, T., Powell, M., Knochenmuss, R., Vertes, A.: Nanophotonic ion production from silicon microcolumn arrays. *Angew. Chem. Inter. Ed.* **48**, 1669–1672 (2009)
- Luo, G.H., Chen, Y., Daniels, H., Dubrow, R., Vertes, A.: Internal energy transfer in laser desorption/ionization from silicon nanowires. *J. Phys. Chem. B* **110**, 13381–13386 (2006)
- Piret, G., Drobacq, H., Coffinier, Y., Melnyk, O., Boukherroub, R.: Matrix-free laser desorption/ionization mass spectrometry on silicon nanowire arrays prepared by chemical etching of crystalline silicon. *Langmuir* **26**, 1354–1361 (2010)
- Finkel, N.H., Prevo, B.G., Velev, O.D., He, L.: Ordered silicon nanocavity arrays in surface-assisted desorption/ionization mass spectrometry. *Anal. Chem.* **77**, 1088–1095 (2005)
- Xiao, Y.S., Retterer, S.T., Thomas, D.K., Tao, J.Y., He, L.: Impacts of surface morphology on ion desorption and ionization in desorption ionization on porous silicon (DIOS) mass spectrometry. *J. Phys. Chem. C* **113**, 3076–3083 (2009)
- Wang, Y.D., Lu, N., Xu, H.B., Shi, G., Xu, M.J., Lin, X.W., Li, H.B., Wang, W.T., Qi, D.P., Lu, Y.Q., Chi, L.F.: Biomimetic corrugated

- silicon nanocone arrays for self-cleaning antireflection coatings. *Nano Res.* **3**, 520–527 (2010)
31. Xu, H.B., Lu, N., Qi, D.P., Hao, J.Y., Gao, L.G., Zhang, B., Chi, L.F.: Biomimetic antireflective Si nanopillar arrays. *Small* **4**, 1972–1975 (2008)
 32. Chen, Y.F., Chen, H.Y., Aleksandrov, A., Orlando, T.M.: Roles of water, acidity, and surface morphology in surface-assisted laser desorption/ionization of amino acids. *J. Phys. Chem. C* **112**, 6953–6960 (2008)
 33. Lu, Y., Lal, A.: High-efficiency ordered silicon nano-conical-frustum array solar cells by self-powered parallel electron Lithography. *Nano Lett.* **10**, 4651–4656 (2010)
 34. Chen, Y., Xu, Z., Gartia, M.R., Whitlock, D., Lian, Y., Liu, G.L.: Ultrahigh throughput silicon nanomanufacturing by simultaneous reactive ion synthesis and etching. *ACS Nano* **5**, 8002–8012 (2011)
 35. Chen, Y., Vertes, A.: Adjustable fragmentation in laser desorption/ionization from laser-induced silicon microcolumn arrays. *Anal. Chem.* **78**, 5835–5844 (2006)